Engineered Regeneration 3 (2022) 387–396

Contents lists available at ScienceDirect

Engineered Regeneration

journal homepage: http://www.keaipublishing.com/en/journals/engineered-regeneration/

# Urinary analysis based on surface-enhanced Raman scattering for the noninvasive screening of lung cancer

Xueqian Ren[a,b], Liping Huang[a], Chengde Wang[c], Yuancai Ge[a], Kaili Zhang[d], Danfeng Jiang[a,b], Xiaohu Liu[a], Qingwen Zhang[a,b,*], Yi Wang[a,b,d,*]

[a] School of Biomedical Engineering, School of Ophthalmology and Optometry, Eye Hospital, Wenzhou Medical University, Wenzhou 325001, China
[b] Engineering Research Center of Clinical Functional Materials and Diagnosis & Treatment Devices of Zhejiang Province, Wenzhou Institute, University of Chinese Academy of Sciences, Wenzhou 325001, China
[c] The First Affiliated Hospital, Wenzhou Medical University, Wenzhou 325001, China
[d] School of Opto-Electronic Engineering, Changchun University of Science and Technology, Changchun 130022, China

ARTICLE INFO

*Keywords:*
Adenosine
Surface-enhanced Raman scattering
Gold nanoparticles
OPLS-DA
Lung cancer
Noninvasive diagnosis

ABSTRACT

We developed a reliable simple analysis of adenosine, creatinine and other nucleosides (cytidine and guanosine) with single measurement based on surface-enhanced Raman spectroscopy (SERS) using DSP-AuNPs with $Cu^{2+}$ ions probe and applied it to achieve noninvasive screening of lung cancer. The gold nanoparticles (AuNPs) were modified with 3,3′-dithiodipropionic acid di (N-hydroxysuccinimide ester) (DSP), which could react with above mentioned molecules followed with the aggregation of AuNPs at the presence of $Cu^{2+}$, thus form the plasmonic hot spots to dramatically increase their fingerprint Raman signal. The probe of DSP-AuNPs was applied for the detail analysis of urinary adenosine of healthy people and lung cancer patients. The SERS measurement indicated a higher concentration of urinary adenosine for lung cancer patients than that of healthy people, which was consistent with the results measured by high-performance liquid chromatography (HPLC). In combination of Raman spectroscopy with the orthogonal partial least squares discriminant analysis (OPLS-DA) model, we are able to discriminate the lung cancer patients from healthy people with the urinary test. The results indicated that besides of adenosine, other metabolites including uric acid, guanine and creatinine may also be the potential tumor markers in urine for the noninvasive lung cancer diagnosis. Such a method paves a way for the noninvasive cancer screening and it can be further modified for the detection of other molecules on medical diagnosis.

## 1. Introduction

Adenosine regulates many important metabolism and functions of the human body as an endogenous purine nucleoside substance. It is considered as a regulator in the brain to protect nerves [1]. In the cardiovascular system, adenosine regulates the formation of new blood vessels, coronary artery vasodilation, and myocardial oxygen demand [2, 3]. In the lungs, adenosine regulates pulmonary microvascular production [4]. The level of extracellular adenosine is very low under physiological conditions, which increased significantly under a variety of stress conditions, such as inflammation, ischemia, and hypoxia [5,6]. However, tumors usually suffer from hypoxia and ischemia due to their rapid growth and metabolism, resulting in an increase of adenosine concentration in solid tumor tissue typically lung cancer [7]. Therefore, adenosine is also considered as a tumor marker for the monitoring of cancer progression [8]. Under the influence of bad eating habits, genetics, environment, and other factors, the number of people with lung cancers has gradually increased in recent years, and lung cancer is the leading cause of death in the global cancer population [9]. Compared with normal people, lung cancer patients have higher levels of adenosine in urine [10–14]. Therefore, providing information on changes in adenosine concentration of urine is of great significance and convenient in the diagnosis, treatment, and prognosis of lung cancer. Common methods for detecting urinary adenosine typically include high-performance liquid chromatography (HPLC) [15,16], gas/liquid chromatography-mass spectrometry [17,18], and fluorescence analysis [19,20]. HPLC and gas/liquid chromatography-mass spectrometry analysis methods are limited by time-consuming and complicated pretreatment procedures. Fluorescence analysis has problems such as autofluorescence and photodegradation. As compared with other traditional analysis methods, surface-enhanced Raman scattering (SERS) has shown great advantages in the detection of adenosine [10,21,22].

SERS is considered a noninvasive technology that offers the selectivity of Raman spectroscopy and the high sensitivity for the detection of biomolecules at ultra-low concentrations [23]. It is widely used in

* Corresponding authors.
*E-mail addresses:* zhangqw@wiucas.ac.cn (Q. Zhang), wangyi@wiucas.ac.cn (Y. Wang).

https://doi.org/10.1016/j.engreg.2022.08.004
Received 13 July 2022; Received in revised form 18 August 2022; Accepted 18 August 2022
Available online 20 August 2022

various fields such as biochemistry, clinical medicine, and materials science [24,25]. Moreover, the SERS signal of the targeted molecules can be remarkably enhanced at the plasmonic hot-spots of the nanostructures such as nanoparticles [26,27], nanorods [28], and nanostars [29], which induces the achievement of single molecular detection [30,31]. Gold nanoparticles (AuNPs) as a promising functional nanomaterial that has already attracted widespread attention in recent years, owing to the excellent optical properties [32–34]. It has been functionalized with different molecules for the detection of specific analytes through colorimetric responses [35,36], electrochemical [37], fluorescence resonance energy transfer [38], and SERS [39,40]. Especially in the SERS analysis, specific analytes which triggered the aggregation of functionalized AuNPs can be significantly enhanced on their SERS signal due to the formation of plasmonic hot-spots [39,41]. Previous mentioned adenosine sensor based on SERS technology and composite nanoparticles, typically required the pretreatment of urine samples before measurements by removal of urea for minimal interference through azo reaction by HCl and $NaNO_2$ [10], extraction of adenosine from urine by affinity chromatography [21], or preconcentration of analyte and pH adjustment of urine to pH=1 [22]. These pretreatment procedures increased the complexity of urinary analysis. In addition, there is few works addressing the SERS measurement of adenosine from patients' urine for cancer diagnosis. Therefore, it is necessary to have a simple and fast SERS platform that does not require complicated sample pre-treatment on the detection of urinary adenosine from clinical samples for non-invasive screening of lung cancer.

In this work, we developed the SERS AuNPs probes for the detection of adenosine, creatinine and other nucleosides (cytidine and guanosine), and further applied it for the noninvasive screening of lung cancer based on the urinary test. The AuNPs were modified with 3,3′-dithiodipropionic acid di (N-hydroxysuccinimide ester) (DSP), which can specifically react with the primary amine group of adenosine and other two nucleosides (guanine and cytidine), thus inducing the aggregation of AuNPs at the presence of $Cu^{2+}$ (Scheme 1). Therefore, the SERS signal of the nucleosides can be significantly enhanced due to the formation of plasmonic hot-spots where the nucleosides are located. The AuNPs were further applied on urinary analysis for the SERS discrimination of healthy people and lung cancer patients in the combination with the orthogonal partial least squares discriminant analysis (OPLS-DA).

## 2. Experimental section

### 2.1. Materials and reagents

Adenosine, Iron (III) chloride hexahydrate, and 3,3′-Dithiodipropionic acid di (N-hydroxysuccinimide ester) (DSP) were purchased from Sigma-Aldrich. Gold (III) chloride trihydrate ($HAuCl_4 \cdot 3H_2O$), trisodium citrate dihydrate, adenosine triphosphate (ATP), adenosine diphosphate (ADP), adenosine monophosphate (AMP), urea, thymidine (T), cupric sulfate anhydrous, magnesium sulfate anhydrous, manganese chloride, iron (II) chloride, uric acid (UA), phenylalanine (Phe), calcium nitrate tetrahydrate, sodium bicarbonate and sodium acetate anhydrous were obtained from Macklin (Shanghai, China). Guanosine (G), cytidine (C), creatinine (Cr), uridine (U), and sodium carbonate anhydrous were obtained from Aladdin (Shanghai, China). Sodium dihydrogen phosphate dihydrate and disodium hydrogen phosphate dodecahydrate were obtained from Guangzhou Jinhuada Chemical Reagent Co., Ltd (Guangdong, China). All the reagents were used as received without further purification. Ultrapure water (≥18 MΩ cm) was produced from ULUPURE system (Sichuan ULUPURE Ultrapure Technology Co., Ltd., Sichuan, China). Phosphate buffered saline (PBS, pH 7.4, 10 mM) consisted of 24% sodium dihydrogen phosphate dihydrate (10 mM) and 76% disodium hydrogen phosphate dodecahydrate (10 mM). Urine samples of lung cancer patients and healthy people were collected and used under the guidelines approved by the Ethics Committee of the Eye Hospital of Wenzhou Medical University (IRB No.2021216).

### 2.2. Preparation of DSP-AuNPs for the detection of adenosine

The AuNPs (22 nm) were functionalized with DSP through a ligand-exchange reaction as we reported previously [41]. 2.5 μL of DSP solution (2 mM) was added into 4 mL AuNPs (3.2 nM) and stirred at room temperature for 45 min. Then, the DSP-AuNPs were centrifuged at 8000 r $min^{-1}$ for 10 min and resuspended in Phosphate buffered saline (PBS, pH 7.4, 10 mM).

For the detection of adenosine in PBS, a volume of 3 μL adenosine at different concentrations (0 mM, 0.05 mM, 0.125 mM, 0.25 mM, 0.375 mM, 0.5 mM, 1 mM, 2.5 mM, 5 mM and 7.5 mM) in PBS and 15 μL $CuSO_4$ solution (1.45 mM) were added into 1.482 mL of DSP-AuNPs and incubated for 45 min at room temperature. The AuNPs were measured by UV–vis, DLS measurement and Raman spectroscopy to characterize the sensor performance. The Raman spectra were implemented by Renishaw Raman system and performed under the condition of 17 mW He-Ne laser (633 nm), L50 × objective lens and integration time of 10 s.

### 2.3. HPLC analysis of adenosine in urine

The HPLC technology was employed for the investigation of adenosine in urine as reported previously [10]. The HPLC analyzer was equipped with a C18 column and a 260 nm ultraviolet detector, while the column temperature was maintained at 30 °C. The mobile phase consisted of 80% ammonium acetate (5 mM, pH = 5) and 20% methanol at a flow rate of 0.8 mL $min^{-1}$. The urine samples from healthy volunteers and lung cancer patients were centrifuged at 11,000 r $min^{-1}$ for 20 min, and then filtered through a 0.22 μm filter membrane. The urine samples were then added into the bottle and pumped into the HPLC analyzer with an injection volume of 5 μL.

### 2.4. SERS analysis of urine

Similarly, urine sample was first centrifuged and filtered through filter membrane as the above HPLC analysis. Subsequently, 20 μL of urine sample and 4 μL of $CuSO_4$ solution (1.45 mM) were added into 76 μL of DSP-AuNPs (12 nM), followed by incubation for 10 min at room temperature. For the detection of adenosine spiked in urine samples, 20 μL of urine sample spiked with adenosine (at different concentrations of 0 μM, 10 μM, 50 μM, 100 μM, 250 μM and 500 μM), and 4 μL of $CuSO_4$ solution (1.45 mM) were added into 76 μL of DSP-AuNPs (12 nM), followed by incubation for 10 min at room temperature. Then, the solution was dropped on the silicone substrate for SERS measurement. The Raman spectra were obtained by Renishaw Raman system and performed under the condition of 17 mW He-Ne laser (633 nm), L50 × objective lens and integration time of 10 s.

## 3. Results and discussion

### 3.1. Characterization of the DSP-AuNPs with $Cu^{2+}$ ions probes

The absorbance peak of AuNPs appeared at 520.6 nm from the UV–vis spectrum (Fig. 1a, black curve, and Figure S1), indicating the nanoparticle size of about 22 nm as shown in the DLS measurement (Figure S2) [42]. The UV–vis spectra showed the absorbance peak of AuNPs red-shifted to 520.7 nm after the modification with DSP (Fig. 1a). The red-shift of 0.1 nm on the absorbance peak is mainly due to the small molecules of DSP (Mw = 202 Da) which replace the citrate (Mw = 189 Da) on the AuNPs thus inducing small changes on the refractive index around the AuNPs. Similar results can be found in the reported AuAg alloy nanoparticles upon modification with different sizes of molecules [36]. The DSP molecules on the AuNPs served as a stabilizer, as well as a specific reaction site for the primary amine group from

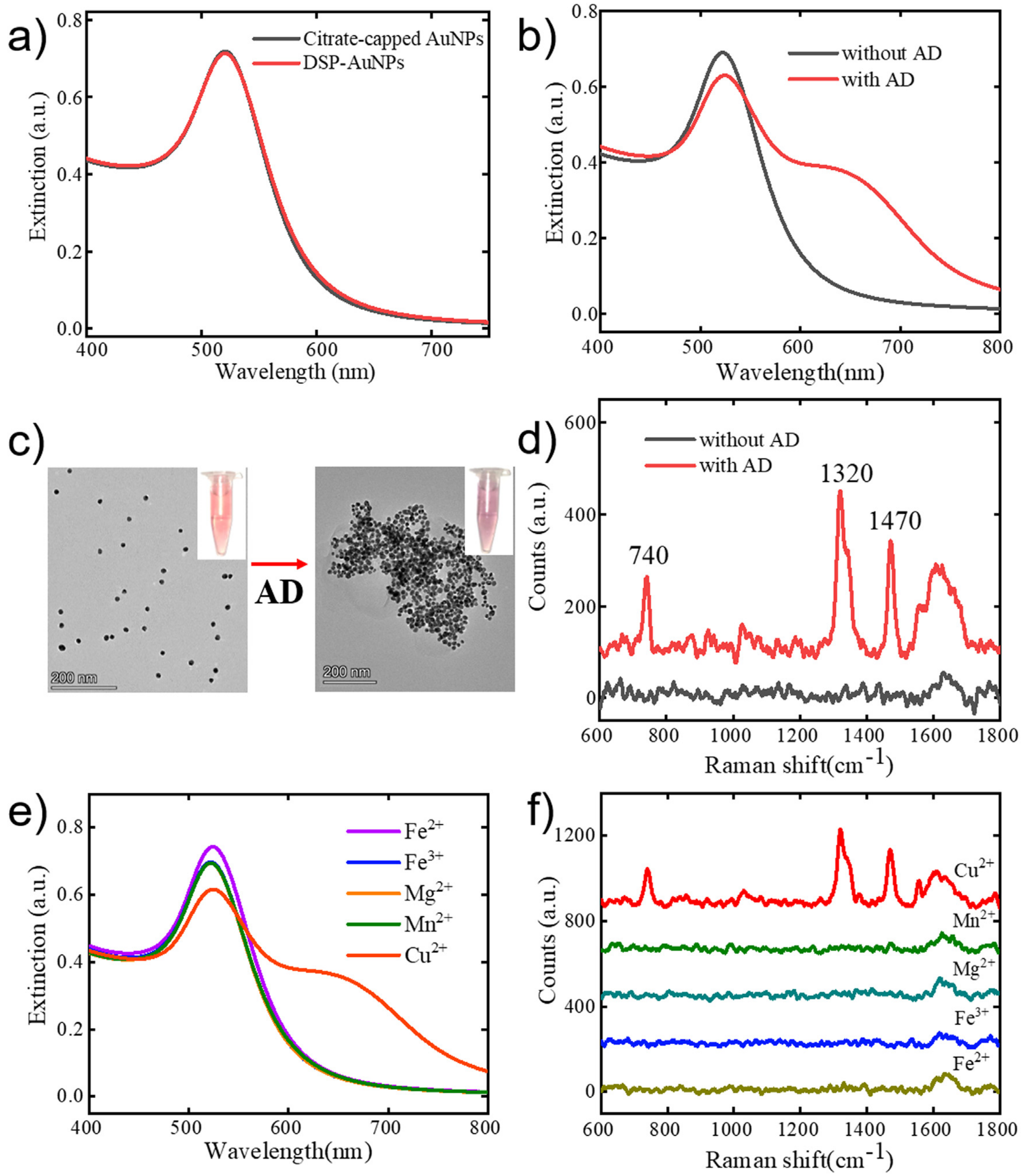


**Fig. 1.** a) UV–vis spectra of the citrate-capped AuNPs and DSP-AuNPs. b) UV–vis spectra of the DSP-AuNPs with $Cu^{2+}$ ions probes before (black line) and after (red line) addition of adenosine (AD) (750 nM). c) Corresponding colors and TEM images of the AuNPs with $Cu^{2+}$ solutions before and after addition of AD in b). Scale bar: 200 nm. d) SERS spectra of the DSP-AuNPs with $Cu^{2+}$ ions probes before (black line) and after (red line) addition of AD (750 nM). e) The UV–vis absorption spectra and (f) Raman spectra of DSP-AuNPs after incubation with 750 nM AD at the presence of different metal ions including $Cu^{2+}$, $Fe^{2+}$, $Fe^{3+}$, $Mn^{2+}$and $Mg^{2+}$, respectively.

nucleosides such as adenosine, guanine and cytidine, which can further react with the $Cu^{2+}$ ions through the *cis* diol interactions, thus resulting in the aggregation of AuNPs (Scheme 1). Upon the addition of 750 nM adenosine at the presence of $Cu^{2+}$ ions (14.5 $\mu$M), the absorbance of DSP-AuNPs showed a decrease at peak wavelength and increase significantly at around 650 nm due to the adenosine induced aggregation of AuNPs (Fig. 1b). We also observed the color of DSP-AuNPs solution changed from wine red to purple, indicating the significant aggregation of AuNPs as shown in the TEM images (Fig. 1c). The DLS measurements also indicated the increase of average diameter of AuNPs up to 80 nm upon 45 min incubation with adenosine at the presence of $Cu^{2+}$ (Figure S3).

Furthermore, the Raman spectra of the DSP-AuNPs probes showed the enhanced Raman intensity at 740 $cm^{-1}$, 1321 $cm^{-1}$ and 1470 $cm^{-1}$ upon the addition of adenosine (Fig. 1d), which was corresponding to the vibration of C–C, C–N and imidazole ring of adenosine, respectively [43]. The control experiment was implemented with the same DSP-AuNPs probe at the absence of $Cu^{2+}$ ions, which showed negligible changes after the incubation of 750 nM adenosine in the UV–vis spectra (Figure S4a) and SERS spectra (Figure S4b), respectively. The above results indicated the aggregation of DSP-AuNPs triggered by adenosine has occurred with the presence of $Cu^{2+}$ ions, which coordinated with the diol of adenosine. To evaluate the specificity of $Cu^{2+}$ ions to adenosine, the DSP-AuNPs were incubated with 750 nM adenosine as well as other

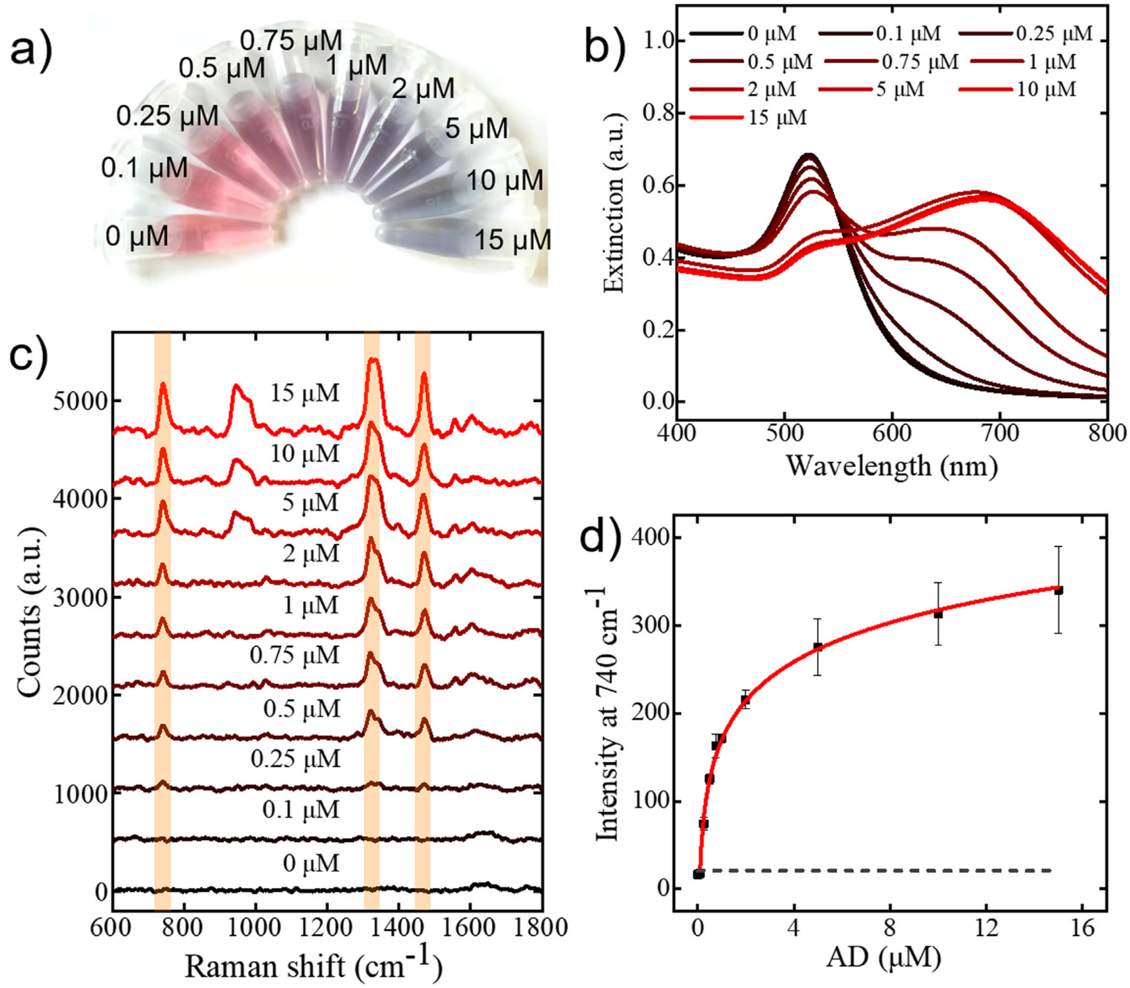


**Fig. 2.** a) The photograph of DSP-AuNPs solutions upon the addition of adenosine at different concentrations from 0 $\mu$M, 0.1 $\mu$M, 0.25 $\mu$M, 0.5 $\mu$M, 0.75 $\mu$M, 1 $\mu$M, 2 $\mu$M, 5 $\mu$M, 10 $\mu$M to 15 $\mu$M, respectively. The corresponding b) UV–vis spectra and c) SERS spectra of the DSP-AuNPs upon the incubation with different concentrations of adenosine. d) The SERS intensity response at 740 $cm^{-1}$ versus the concentrations of adenosine, while the dashed line indicated the noise level, i.e. the signal of blank sample plus 3 times the standard deviation.

metal ions including $Fe^{2+}$, $Fe^{3+}$, $Mn^{2+}$ and $Mg^{2+}$ ions (at the presence of $FeCl_2$, $FeCl_3$, $MnCl_2$ and $MgSO_4$) for 45 min, respectively. As shown in Fig. 1e, there are no obvious changes in the UV–vis spectra of the DSP-AuNPs for the other metal ions ($Fe^{2+}$, $Fe^{3+}$, $Mn^{2+}$, $Mg^{2+}$) as compared with that for $Cu^{2+}$ ions due to the lack of *cis* diol interactions with adenosine. In addition, the SERS spectra of DSP-AuNPs probes showed a negligible signal of adenosine at the presence of other metal ions instead of $Cu^{2+}$ ions (Fig. 1f). Furthermore, the probes also showed negligible SERS response of adenosine at the presence of anions including $Cl^-$, $SO_4{}^{2-}$, $H_2PO_4{}^-$ and $HPO_4{}^{2-}$ (components of PBS buffer), $CO_3{}^{2-}$, $HCO_3{}^-$, $CH_3COO^-$ and $NO_3{}^-$ (Figure S5). The results indicated the good specificity of $Cu^{2+}$ ions for the interaction with adenosine and the validity of the DSP-AuNPs probes for the detection of adenosine.

In addition, the responses of adenosine at the presence of different concentrations of $Cu^{2+}$ (0 $\mu$M, 1 $\mu$M, 5 $\mu$M, 10 $\mu$M, 14.5 $\mu$M, 20 $\mu$M and 50 $\mu$M) were also investigated (Figure S6a). The SERS spectra showed a negligible response to adenosine (0.75 $\mu$M) at the presence of a low concentration of $Cu^{2+}$ (1 $\mu$M). However, the Raman response increased with the concentration of $Cu^{2+}$ and reached a plateau when the concentration increased higher than 14.5 $\mu$M (Figure S6b). Therefore, the concentration of $Cu^{2+}$ at 14.5 $\mu$M was applied on the following assay. Furthermore, to have the high sensitivity, the reaction kinetics of DSP-AuNPs with adenosine at the presence of $Cu^{2+}$ were investigated by UV–vis absorption spectra, DLS and Raman spectra as shown in Figure S7. The UV–vis absorption spectra showed the value of A650/521 increased gradually during the 90 min incubation (Figure S7a and S7b). The response at 45 min was about 90% of that at 90 min. In addition, the DLS measurements showed the size of AuNPs increased significantly during the first 45 min incubation and reached a slow increase during the last 45 min incubation (Figure S7c and S7d). The SERS intensity at 740 $cm^{-1}$, 1321 $cm^{-1}$ and 1470 $cm^{-1}$ showed the maximal response at 45 min incubation and decreased by about 10% of the maximal response after another 45 min reaction (Figure S7e and S7f). The decrease of the response might be ascribed to the precipitation of AuNPs during aggregation which induces a reduced number of nanoparticles in the solution thus the lower Raman intensity. Therefore, the incubation time of 45 min was considered for the following assay.

### 3.2. Sensitivity and selectivity for AD detection

To further investigate the sensitivity for the detection of adenosine, different concentrations of adenosine (0 ~ 15 $\mu$M) were incubated with the DSP-AuNPs probes at the presence of $Cu^{2+}$ ions (14.5 $\mu$M). The color of DSP-AuNPs changed from red, purple to blue with the increased concentration of adenosine owing to the increased amount of particles aggregation (Fig. 2a). Note that the color showed significant differences when the concentration of adenosine reached higher than 0.5 $\mu$M (Fig. 2a). The DLS measurements of the DSP-AuNPs probes also showed

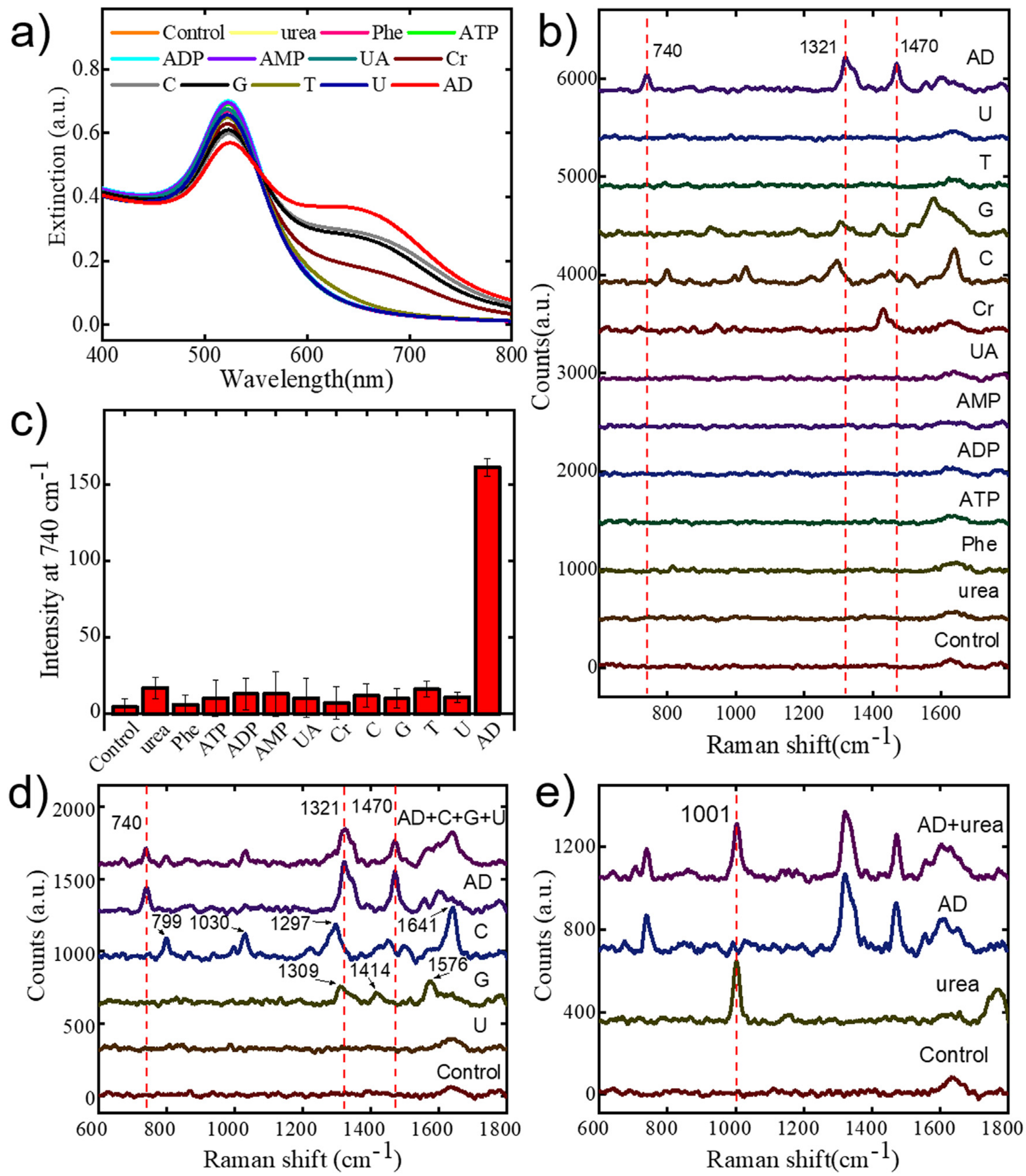


**Fig. 3.** a) The UV–vis spectra, and b) the Raman spectra of DSP-AuNPs upon addition of 0.75 μM of different molecules (urea, Phe, ATP, ADP, AMP, UA, G, C, Cr, U, T and adenosine (AD)). c) The histogram of Raman intensities at 740 cm$^{-1}$ in the presence of adenosine and different interference biomolecules at 0.75 $\mu$M, corresponding to the data in b. Error bars represent the standard deviations of three independent measurements. d) The Raman spectra of the SERS probes before and after incubation with 4 different nucleosides (U, G, C, adenosine) at 0.75 μM, as well as the mixture of 4 nucleosides. e) SERS spectra of the probes before and after incubation with urea (0.3 M), adenosine (0.75 μM) and the mixture of urea (0.3 M) and adenosine (0.75 μM).

a significant increase of average diameter up to about 450 nm (Figure S8a and S8b). The UV–vis spectra of the DSP-AuNPs probes showed the absorbance intensity decreased at the peak wavelength of 521 nm and gradually increased at around 650~700 nm upon increasing the concentration of adenosine (Fig. 2b), which had great correlations as the color changes. The calibration curve was plotted according to the ratio of absorbance intensity at 650 nm and 521 nm (A650/A521) versus the concentrations of adenosine, which shows the limit of detection (LOD) of 0.1 μM for the detection of adenosine based on the UV–vis spectra (Figure S9a). Moreover, the SERS measurement showed the intensity increase at 740 cm$^{-1}$, 1321 cm$^{-1}$ and 1470 cm$^{-1}$ along with the increased concentration of adenosine (Fig. 2c). The calibration curve was also plotted according to the SERS intensity at 740 cm$^{-1}$, which shows the LOD of 0.1 $\mu$M. The LOD was determined as the concentration of analyte where the response is about the signal of blank sample plus 3 times of the standard deviation (dashed line in Fig. 2d), which was comparable with the colorimetric result. The SERS intensity at 1321 cm$^{-1}$ and 1470 cm$^{-1}$ versus the concentration of adenosine also showed the comparable LOD as 0.166 μM and 0.145 μM, respectively (Figure S9b, S9c). Note that the LOD might be further improved by optimizing the size, materials and shapes of nanoparticles. For instance, large nanoparticles up to 68 nm may provide higher Raman signal as compared with small AuNPs (Figure S10 and S11), however, the current LOD based on 22 nm AuNPs is sufficient for the detection of adenosine in urine sam-

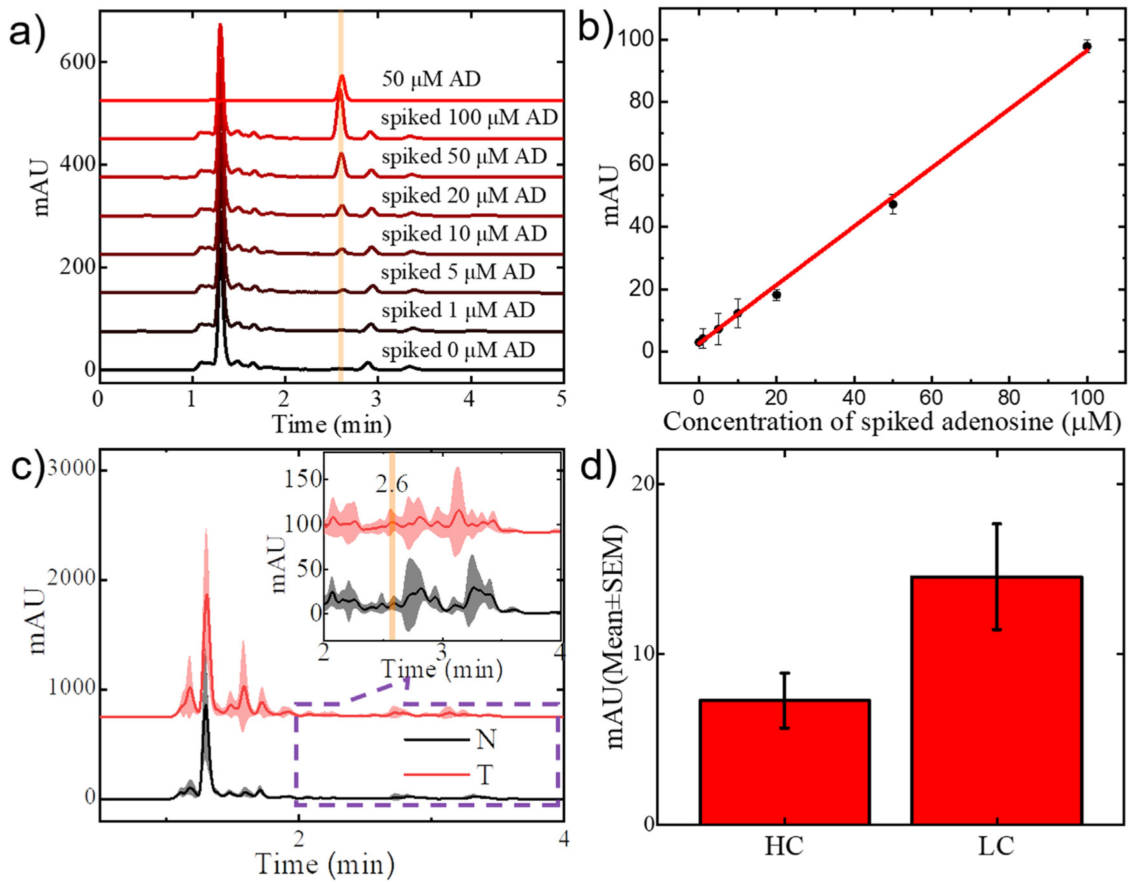


**Fig. 4.** a) HPLC analysis of adenosine aqueous solution (50 μM) and human urine spiked with different concentrations of adenosine from 0 μM, 1 μM, 5 μM, 10 μM, 20 μM, 50 μM, to 100 μM respectively. b) The HPLC peak intensity at the retention time of 2.6 min versus the urine sample spiked with different concentrations of adenosine. Error bars represent the standard deviation of multiple independent measurements ($n \geq 3$). c) The average HPLC signal of urine samples from HC groups ($n = 10$) and LC groups ($n = 10$), respectively. d) The average peak intensity at the retention time of 2.6 min for the HC groups ($n = 10$) and LC groups ($n = 10$), respectively. Error bars represent the standard deviation of multiple independent measurements ($n = 10$).

ples (typically with adenosine of 4 μM to 50 μM). In addition, to avoid the easy sedimentation of large nanoparticles upon small aggregations, we stuck at 22 nm AuNPs probes for further applications.

The selectivity of the SERS probes for adenosine detection was then evaluated by incubating the nanoprobes with various biomolecules (0.75 $\mu$M) including adenosine triphosphate (ATP), adenosine diphosphate (ADP), adenosine monophosphate (AMP), urea, phenylalanine (Phe), uric acid (UA), guanosine (G), cytidine (C), creatinine (Cr), uridine (U), thymidine (T) and adenosine (AD) for 45 min, respectively (Figure S12a). The results showed that adenosine could induce the most significant color changes in the colloidal solution (Figure S12b). However, C and G have functional groups of the amino group and diol group similar to adenosine (Figure S13), which also caused the weak color changes due to the molecules caused partial aggregations of DSP-AuNPs probes (Figure S12b). The UV–vis spectra further showed that adenosine caused the most significant increase of A650/A521 value as compared with other biomolecules, while the A650/A521 values for C and G were over half of that produced by adenosine (Fig. 3a and S12a). The results indicated that the colorimetric assay showed weak selectivity for the detection of adenosine. However, the SERS analysis of these biomolecules exhibited the significantly different Raman spectra that the adenosine showed the Raman peaks at 740 cm$^{-1}$, 1321 cm$^{-1}$ and 1470 cm$^{-1}$, while the other biomolecules including C, G, U and T didn't show any Raman peaks at 740 cm$^{-1}$ (Fig. 3b). A histogram based on the peak intensity at 740 cm$^{-1}$ for all the biomolecules was concluded in Fig. 3c, which indicated the high specificity of this probe for SERS detection of adenosine. Furthermore, the four nucleosides (all at 0.75 $\mu$M) including C, G, U and adenosine exhibited their unique SERS spectra owing to their different molecular structures. As shown in Fig. 3d, cytidine (C) shows the unique SERS peaks at 799 cm$^{-1}$, 1030 cm$^{-1}$, 1297 cm$^{-1}$ and 1641 cm$^{-1}$, while guanosine (G) shows the unique peak at 1309 cm$^{-1}$, 1414 cm$^{-1}$ and 1576 cm$^{-1}$. In addition, the mixing solution of the four nucleosides at the same concentration were incubated with the nanoprobes to investigate their interference on the SERS probes. The results indicated that their characteristic peaks can be easily observed in one spectrum including the adenosine Raman peak at 740 cm$^{-1}$ (Fig. 3d), indicating that the SERS probes can specifically identify adenosine from the other three nucleosides. The result indicated the advantage of SERS method for the distinguish of different molecules based on their fingerprint spectra which is not feasible for the colorimetric method especially if there are interferents. Note that these probes may pave a way for future application on the detection of the four nucleosides at the same time with the single assay.

In addition, considering the further application on the detection of adenosine detection in human urine, in which the urea concentration is usually high up to 0.3 M [10,44], which is about 2–3 orders of magnitude higher than the concentration of adenosine. Therefore, the interference of urea to the detection of adenosine was further investigated by incubation of the urea, and the mixture of adenosine and urea with the DSP-AuNPs probes, respectively. As shown in Fig. 3e, the characteristic peak of urea appeared at 1001 cm$^{-1}$ in the SERS spectrum, which did not overlap with any of the characteristic peaks of adenosine (740 cm$^{-1}$, 1321 cm$^{-1}$ and 1470 cm$^{-1}$). In addition, the urea (0.3 M) spiked with adenosine (0.75 $\mu$M) showed both the obvious SERS peaks of adenosine

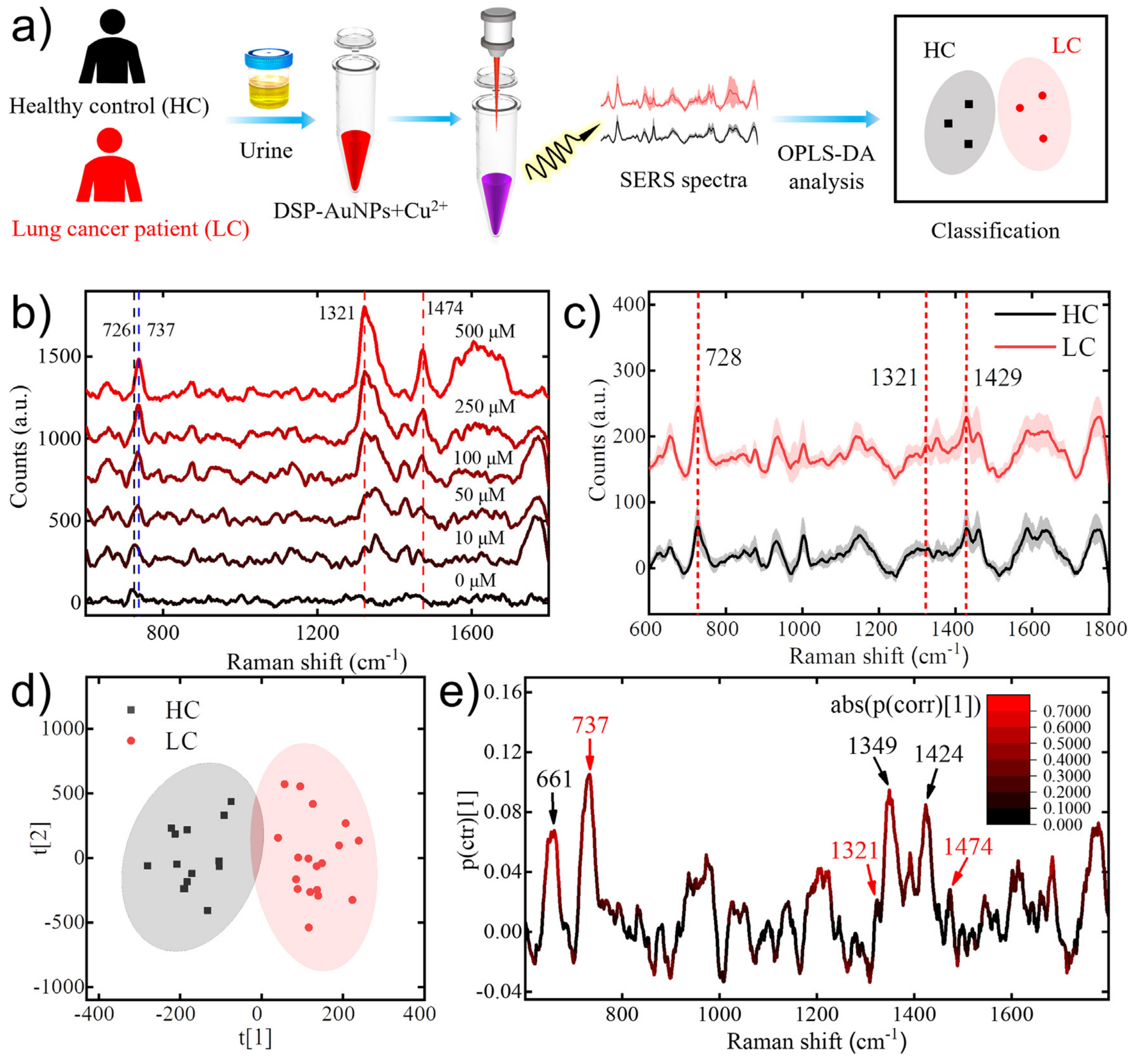


**Fig. 5.** a) Schematic illustration for the SERS probes applied for HC and LC measurement, followed with OPLS-DA analysis for the classification of the two groups. b) SERS spectra of the probes incubated with the urine samples before and after spiked with different concentrations of adenosine from 0 to 500 μM. c) The SERS spectra and their averages from the urine samples of HC groups ($n$ = 14) and LC groups ($n$ = 18), respectively. d) The OPLS-DA score plot of HC groups (square) and LC groups (circle). Ellipse: Hotelling's T2 (95%). e) The S-line plot based on the OPLS-DA models for LC groups (positive) and HC groups (negative), where 737 $cm^{-1}$, 1321 $cm^{-1}$ and 1474 $cm^{-1}$ were assigned to adenosine.

and urea (Fig. 3e). The results indicated that the presence of a high concentration of urea has a negligible effect on the detection of adenosine.

### 3.3. Detection of adenosine in urine

For the further detection of adenosine in human urine, the HPLC experiments were employed to evaluate the level of adenosine in urine. The adenosine aqueous solution (1 mM) was used as a reference [10], which showed the significant signal at the retention time of 2.6 min as measured by HPLC (Fig. 4a). The urine samples from healthy controls (HC) spiked with different concentrations of adenosine were measured under the same experimental condition by HPLC, which also demonstrated the retention time of 2.6 min (Fig. 4a). The chromatographic peak intensity at 2.6 min increased gradually upon increasing the concentration of spiked adenosine (from 1 $\mu$M to 100 $\mu$M) in urine samples (Fig. 4a). The results showed a linear relationship between the spiked adenosine concentration and the chromatographic peak intensity at 2.6 min, with a function as $y = 0.94\ (x\text{-}c) + 2.6$ (with $R^2 = 0.9979$) (Fig. 4b), where $c$ is considered as the original concentration of adenosine in the HC urine, and $x$-$c$ is the concentration of spiked adenosine. The concentration in this HC urine was estimated as $c = 2.77$ $\mu$M, assuming the intercept of the curve goes to 0 (i.e. the peak intensity is 0 in the absence of adenosine). Furthermore, the urine samples from 10 lung cancer patients (LC) and 10 healthy controls were analyzed by HPLC, which showed the difference of the average HPLC signals for LC and HC groups (Fig. 4c). The chromatographic peak intensity of urine adenosine at 2.6 min was higher for the LC patients than that for HC group. According to the above function deduced from Fig. 4b, the average concentrations of urinary adenosine were evaluated as about 7.75 $\mu$M and 15.48 $\mu$M for the HC and LC group, respectively (Fig. 4d). The results were comparable with the reported concentration of urinary adenosine of 7 $\mu$M for healthy people [45,46]. In addition, the concentration of urinary adenosine in lung cancer patients was higher than that of healthy people, which was also consistent with the results previously reported [47].

### 3.4. Noninvasive screening of lung cancer

In addition, the SERS strategy was accordingly applied for adenosine detection in urine from LC and HC groups and analyzed for the classification (Fig. 5a), given that the concentration of urinary adenosine was approximate between 4 $\mu$M and 50 $\mu$M [45,47]. Note that the

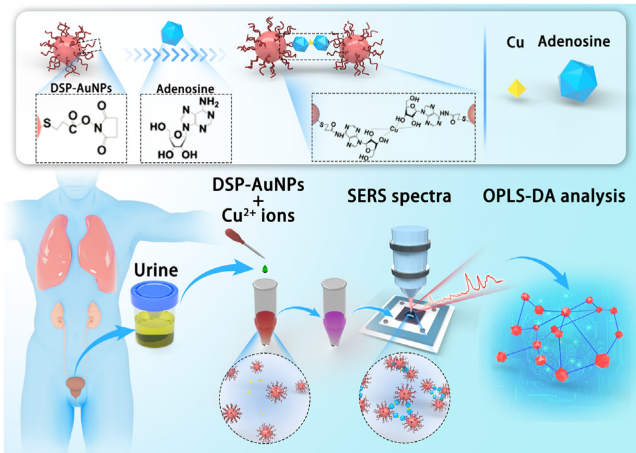


**Scheme 1.** Schematic illustration of adenosine SERS detection strategy based on DSP-AuNPs at the presence of $Cu^{2+}$, and further applied for the noninvasive screening of lung cancer with the OPLS-DA analysis.

urine samples after added into the $CuSO_4$ and DSP-AuNPs solution were essentially diluted by a factor of 5 in this assay, thus the detection range covers the typical concentration of urinary adenosine. To evaluate the feasibility of SERS probes for urinary adenosine detection, urine samples spiked with different concentrations of adenosine (from 0 $\mu$M, 10 $\mu$M, 50 $\mu$M, 100 $\mu$M, 250 $\mu$M and 500 $\mu$M) were incubated with the probes for 10 min before the measurement. The results showed the Raman peak at 726 $cm^{-1}$ of the urine sample separated into two peaks at 726 $cm^{-1}$ and 737 $cm^{-1}$ along with the increased concentration of adenosine (Fig. 5b). The peak at 726 $cm^{-1}$ was considered as the uric acid or hypoxanthine [48,49]. In addition, the Raman intensities at the other two characteristic peaks of adenosine (1321 $cm^{-1}$ and 1474 $cm^{-1}$) were also increased with the concentration of spiked adenosine in urine. The calibration curve was also plotted according to the SERS intensity at 1321 $cm^{-1}$ in urine, which shows the LOD of about 3 $\mu$M (Figure S14). The LOD is lower than the usual urinary adenosine concentration (4 $\mu$M ~ 50 $\mu$M), indicating the feasibility of the SERS nanoprobe applied for the detection of adenosine in urine. However, the Raman peaks position (737 $cm^{-1}$, 1321 $cm^{-1}$, and 1474 $cm^{-1}$) of the adenosine in urine samples have 1–4 $cm^{-1}$ of shifts as that measured in PBS (740 $cm^{-1}$, 1321 $cm^{-1}$ and 1470 $cm^{-1}$). The slight shifts may be attributed to the complicated matrix of urine in which other biomolecules have overlapped Raman signal with the adenosine and/or interfered with the vibration of adenosine. In addition, the SERS measurement of the probes incubated with urine samples from LC group ($n$ = 18) and HC group ($n$ = 14) showed obvious higher average peak intensity at 728 $cm^{-1}$, 1321 $cm^{-1}$, and 1429 $cm^{-1}$ for LC group (Fig. 5c). The detailed information for the 18 LC patients and 14 healthy volunteers were listed in Table S1, S2 and S3, including their gender, ages, tumor location and differentiation, and their urinalysis and blood biomarkers tests results (CEA, CA, Keratin, squamous cell carcinoma antigen, and so on). In addition, the multiple Raman measurements of urine samples from 2 healthy volunteers and 3 LC patients showed good reproducible spectra (Figure S15a) with the average relative standard deviation of 13.8% for the Raman intensity at 728 $cm^{-1}$, 1321 $cm^{-1}$ and 1429 $cm^{-1}$ (Figure S15b). The results indicated the good reproducibility of the assay.

To better discriminate the LC group from HC group, orthogonal partial least squares discriminant analysis (OPLS-DA) was employed to analyze the SERS spectra. OPLS-DA is a multivariate statistical modeling tool, which could reduce the dimensionality of the data to establish a regression model based on methods of partial least squares regression, and perform discriminant analysis for regression results [50]. Moreover, OPLS-DA can conduct orthogonal transformation correction of the data, thus eliminating the noise of unrelated classification information to better obtain critical information of differences among different groups [50]. Based on the OPLS-DA assessment, the LC group can be discriminated from the HC group with one predictive component (t1) and one orthogonal component (t2) (Fig. 5d). The dataset of the two groups was clustered respectively in 95% confidence ellipses, which indicated a statistically significant difference between the two groups. In this model, the variation [$R^2$ Y(cum)] was 0.88 between the two groups, while the variation [$R^2$ X(cum)] was 0.464, and the predictability of the model $Q^2$ (cum) was 0.601, which meant the good robustness and predictability of such model. Additionally, the confusion matrix (misclassification table) and receiver operating characteristic (ROC) curves were conducted to assess the performance of OPLS-DA model. The misclassification table results reflected the overall accuracy of 100% for all tests (Figure S16a). The ROC curves showed that an area under the curve (AUC) value was 1 for the two group samples (Figure S16b). These results indicated the feasibility to discriminate the two group samples by this model.

In addition, the S-line of OPLS-DA for t1 was plotted to further evaluate specific metabolite differences between the two group samples. The covariance (p(ctr)) and correlation coefficient (abs(p(corr)) between the variables and classification score in the model were visualized through the S-line of the OPLS-DA [51]. As shown in Fig. 5e, the S-line of OPLS-DA visualized differences between LC group (positive) and HC group (negative). The absolute value of the variables was high at 661 $cm^{-1}$, 737 $cm^{-1}$, 1349 $cm^{-1}$ and 1424 $cm^{-1}$, and they were assigned to uric acid, adenosine, guanine and creatinine, respectively [49,52]. The results indicated that these molecules especially adenosine had primary contributions to the differentiation of the LC and HC groups. Besides adenosine, the other metabolites such as uric acid and creatinine were also reported with a higher level in urine from LC group [53]. As expected, the model of OPLS-DA confirmed urinary adenosine as a biomarker for lung cancer detection. Overall, the results showed feasibility for the screening of lung cancer based on the SERS probes, and it paves a way for the future noninvasive screening of lung cancer in clinical application after extensive samples analysis.

## 4. Conclusions

We have successfully developed a SERS sensing platform for the highly sensitive and specific detection of adenosine in both PBS and urine. The DSP-AuNPs with $Cu^{2+}$ ions as SERS probe were confirmed in both colorimetric and SERS assays for the detection of adenosine, with the detection limit down to 0.1 μM. The specific study of the probe indicated the feasibility for the detection of four nucleosides (adenosine, guanine, cytidine and uridine) at the same time with the single assay. In addition, the analysis of SERS spectra was carried out with OPLS-DA model for the investigation of urine samples from LC patients and healthy volunteers. It demonstrated that the adenosine concentration in urine of LC patients was higher than that of healthy people, which was consistent with the results measured by HPLC. In combination with OPLS-DA, the SERS measurement showed effectiveness for the noninvasive screening of LC from healthy volunteers based on the urinary analysis. In addition, besides adenosine, the other urinary metabolites such as uric acid and creatinine may also contribute to the main differences of LC patients and healthy volunteers. This method paves a way for the future clinical application on the noninvasive screening of LC based on urinary SERS analysis once extensive clinical urine samples were analyzed. We expect that future work would include the SERS investigation of urine samples from different tumor locations, tumor stages and differentiations of LC to assist the diagnosis and therapy of LC. In addition, upon the modification of SERS probes, it is expected to be employed for the detection and imaging of other biomolecules.

## CRediT author statement

**Xueqian Ren**: Data curation and Writing-Original draft. **Liping Huang** and **Chengde Wang**: Resources. **Yuancai Ge, Kaili Zhang** and

**Danfeng Jiang**: Formal Analysis. **Xiaohu Liu**: Reviewing and Editing draft. **Qingwen Zhang** and **Yi Wang**: Funding acquisition, Conceptualization, Methodology, Writing-Reviewing and editing.

## Supplementary materials

Supplementary material associated with this article can be found, in the online version, at doi:

## Declaration of Competing Interest

The authors declare that they have no known competing financial interests or personal relationships that could have appeared to influence the work reported in this paper.

## Acknowledgments

This work was financially supported by Zhejiang Province Natural Science Fund for Distinguished Young Scholars (LR19H180001), Public Projects of Wenzhou (G2020005) and the Startup Fund of Wenzhou Institute, UCAS (WIUCASQD2021031).

## Supplementary materials

Supplementary material associated with this article can be found, in the online version, at doi:10.1016/j.engreg.2022.08.004.

## References


[1] T.W. Stone, Adenosine, neurodegeneration and neuroprotection, Neurol. Res. 27 (2) (2005) 161–168.
[2] M. Hori, M. Kitakaze, Adenosine, the heart, and coronary circulation, Hypertension 18 (5) (1991) 565–574.
[3] A.B. Reiss, D. Grossfeld, L.J. Kasselman, H.A. Renna, N.A. Vernice, W. Drewes, J. Konig, S.E. Carsons, J. DeLeon, Adenosine and the cardiovascular system, Am. J. Cardiovasc. Drugs 19 (5) (2019) 449–464.
[4] A. Ahmad, S. Ahmad, L. Glover, S.M. Miller, J.M. Shannon, X.L. Guo, W.A. Franklin, J.P. Bridges, J.B. Schaack, S.P. Colgan, C.W. White, Adenosine A(2A) receptor is a unique angiogenic target of HIF-2 alpha in pulmonary endothelial cells, Proc. Natl. Acad. Sci. U. S. A. 106 (26) (2009) 10684–10689.
[5] G. Hasko, L. Antonioli, B.N. Cronstein, Adenosine metabolism, immunity and joint health, Biochem. Pharmacol. 151 (2018) 307–313.
[6] L. Baron, A. Gombault, M. Fanny, B. Villeret, F. Savigny, N. Guillou, C. Panek, M.Le Bert, V. Lagente, F. Rassendren, N. Riteau, I. Couillin, The NLRP3 inflammasome is activated by nanoparticles through ATP, ADP and adenosine, Cell Death Dis 6 (2015).
[7] M. Mujoomdar, D. Hoskin, J. Blay, Adenosine stimulation of the proliferation of colorectal carcinoma cell lines - roles of cell density and adenosine metabolism, Biochem. Pharmacol. 66 (9) (2003) 1737–1747.
[8] J.Q. Zhang, Y.S. Wang, Y. He, T. Jiang, H.M. Yang, X. Tan, R.H. Kang, Y.K. Yuan, L.F. Shi, Determination of urinary adenosine using resonance light scattering of gold nanoparticles modified structure-switching aptamer, Anal. Biochem. 397 (2) (2010) 212–217.
[9] H. Shin, S. Oh, S. Hong, M. Kang, D. Kang, Y.G. Ji, B.H. Choi, K.W. Kang, H. Jeong, Y. Park, S. Hong, H.K. Kim, Y. Choi, Early-stage lung cancer diagnosis by deep learning-based spectroscopic analysis of circulating exosomes, ACS Nano 14 (5) (2020) 5435–5444.
[10] T.X. Yang, X.Y. Guo, Y.P. Wu, H. Wang, S.Y. Fu, Y. Wen, H.F. Yang, Facile and label-free detection of lung cancer biomarker in urine by magnetically assisted surface-enhanced Raman scattering, ACS Appl. Mater. Interfaces 6 (23) (2014) 20985–20993.
[11] S. Zhou, Y. Gan, L. Kong, J. Sun, T. Liang, X. Wang, H. Wan, P. Wang, A novel portable biosensor based on aptamer functionalized gold nanoparticles for adenosine detection, Anal. Chim. Acta 1120 (2020) 43–49.
[12] J. You, Z. You, X. Xu, J. Ji, T. Lu, Y. Xia, L. Wang, L. Zhang, S. Du, A split aptamer-labeled ratiometric fluorescent biosensor for specific detection of adenosine in human urine, Microchimica Acta 186 (1) (2018) 43.
[13] Y. Lu, L. Lin, J. Ye, Human metabolite detection by surface-enhanced Raman spectroscopy, Materials Today Bio. 13 (2022) 100205.
[14] J. Sun, W. Jiang, J. Zhu, W. Li, L. Wang, Label-free fluorescence dual-amplified detection of adenosine based on exonuclease III-assisted DNA cycling and hybridization chain reaction, Biosens. Bioelectron. 70 (2015) 15–20.
[15] A. Andries, S. De Rechter, P. Janssens, D. Mekahli, A. Van Schepdael, Simultaneous determination of allantoin and adenosine in human urine using liquid chromatography - UV detection, J. Chromatogr. B. 1096 (2018) 201–207.
[16] R.A. Altaweraqi, S.Y.M. Yao, K.M. Smith, C.E. Cass, J.D. Young, HPLC reveals novel features of nucleoside and nucleobase homeostasis, nucleoside metabolism and nucleoside transport, Biochim. Biophys. Acta-Biomembr. 1862 (7) (2020) 13.
[17] S.D. Spivack, M. Shi, D. Patel, A. Desai, J.B. Dobkin, C. Shah, D. Hosgood, K. Ye, Y. Qiu, I. Kurland, Exhaled small, polar, energetics-related metabolites by GC-MS for lung cancer risk assessment, Am. J. Respir. Crit. Care Med. 199 (2019) 2.
[18] P. Monostori, G. Klinke, J. Hauke, S. Richter, J. Bierau, S.F. Garbade, G.F. Hoffmann, C.D. Langhans, D. Haas, J.G. Okun, Extended diagnosis of purine and pyrimidine disorders from urine: LC MS/MS assay development and clinical validation, PLoS ONE 14 (2) (2019) 17.
[19] S. Yousefi, M. Saraji, Developing a fluorometric aptasensor based on carbon quantum dots and silver nanoparticles for the detection of adenosine, Microchem J 148 (2019) 169–176.
[20] X.Y. Chen, X.R. Fu, Y.Y. Wu, Y.F. Jin, W. Li, A DNA tweezers-actuated regenerated DNAzyme nanoreactor: a fluorescence sensor for MiRNA and adenosine detection, Anal. Methods 12 (12) (2020) 1579–1586.
[21] S.C. Xu, B.Y. Man, S.Z. Jiang, J.H. Wang, J. Wei, S.D. Xu, H.P. Liu, S.B. Gao, H.L. Liu, Z.H. Li, H.S. Li, H.W. Qiu, Graphene/Cu nanoparticle hybrids fabricated by chemical vapor deposition as surface-enhanced Raman scattering substrate for label-free detection of adenosine, ACS Appl. Mater. Interfaces 7 (20) (2015) 10977–10987.
[22] J.E.L. Villa, C. Pasquini, R.J. Poppi, Surface-enhanced Raman spectroscopy and MCR-ALS for the selective sensing of urinary adenosine on filter paper, Talanta 187 (2018) 99–105.
[23] X.H. Liu, X.M. Liu, P.F. Rong, D.B. Liu, Recent advances in background-free Raman scattering for bioanalysis, Trac-Trends Anal. Chem. 123 (2020) 14.
[24] C. Zong, M.X. Xu, L.J. Xu, T. Wei, X. Ma, X.S. Zheng, R. Hu, B. Ren, Surface-enhanced Raman spectroscopy for bioanalysis: reliability and challenges, Chem. Rev. 118 (10) (2018) 4946–4980.
[25] D. Cialla-May, X.S. Zheng, K. Weber, J. Popp, Recent progress in surface-enhanced Raman spectroscopy for biological and biomedical applications: from cells to clinics, Chem. Soc. Rev. 46 (13) (2017) 3945–3961.
[26] W. Zhu, B.-.Y. Wen, L.-.J. Jie, X.-.D. Tian, Z.-.L. Yang, P.M. Radjenovic, S.-.Y. Luo, Z.-.Q. Tian, J.-.F. Li, Rapid and low-cost quantitative detection of creatinine in human urine with a portable Raman spectrometer, Biosens. Bioelectron. (2020) 154.
[27] K. Koike, K. Bando, J. Ando, H. Yamakoshi, N. Terayama, K. Dodo, N.I. Smith, M. Sodeoka, K. Fujita, Quantitative drug dynamics visualized by alkyne-tagged plasmonic-enhanced Raman microscopy, ACS Nano 14 (11) (2020) 15032–15041.
[28] Y. Wang, X. Zhao, Z. Yu, Z. Xu, B. Zhao, Y. Ozaki, A chiral-label-free SERS strategy for the synchronous chiral discrimination and identification of small aromatic molecules, Angew. Chem.-Int. Edit. 59 (43) (2020) 19079–19086.
[29] J.A. Huang, M.Z. Mousavi, G. Giovannini, Y. Zhao, A. Hubarevich, M.A. Soler, W. Rocchia, D. Garoli, F. De Angelis, Multiplexed discrimination of single amino acid residues in polypeptides in a single SERS hot spot, Angew. Chem.-Int. Edit. (2020).
[30] J. Langer, D.J. de Aberasturi, J. Aizpurua, R.A. Alvarez-Puebla, B. Auguie, J.J. Baumberg, G.C. Bazan, S.E.J. Bell, A. Boisen, A.G. Brolo, J. Choo, D. Cialla-May, V. Deckert, L. Fabris, K. Faulds, F.J.G. de Abajo, R. Goodacre, D. Graham, A.J. Haes, … L.M. Liz-Marzan, Present and future of surface-enhanced Raman scattering, ACS Nano 14 (1) (2020) 28–117.
[31] S.Y. Ding, E.M. You, Z.Q. Tian, M. Moskovits, Electromagnetic theories of surface-enhanced Raman spectroscopy, Chem. Soc. Rev. 46 (13) (2017) 4042–4076.
[32] X.H. Liu, Q.W. Zhang, W.G. Knoll, B. Liedberg, Y. Wang, Rational design of functional peptide-gold hybrid nanomaterials for molecular interactions, Adv. Mater. 32 (37) (2020) 37.
[33] X.H. Liu, Y. Wang, P. Chen, A. McCadden, A. Palaniappan, J.L. Zhang, B. Liedberg, Peptide functionalized gold nanoparticles with optimized particle size and concentration for colorimetric assay development: detection of cardiac troponin I, ACS Sens 1 (12) (2016) 1416–1422.
[34] A. Maus, L. Strait, D. Zhu, Nanoparticles as delivery vehicles for antiviral therapeutic drugs, Eng. Regenerat. 2 (2021) 31–46.
[35] X.H. Liu, Y. Wang, P. Chen, Y.S. Wang, J.L. Mang, D. Aili, B. Liedberg, Biofunctionalized gold nanoparticles for colorimetric sensing of botulinum neurotoxin A light chain, Anal. Chem. 86 (5) (2014) 2345–2352.
[36] P. Chen, X. Liu, G. Goyal, T. Nhung Thi, J.C.S. Ho, Y. Wang, D. Aili, B. Liedberg, Nanoplasmonic sensing from the human vision perspective, Anal. Chem. 90 (7) (2018) 4916–4924.
[37] J.L. Zhang, Y. Wang, T.I. Wong, X.H. Liu, X.D. Zhou, B. Liedberg, Electrofocusing-enhanced localized surface plasmon resonance biosensors, Nanoscale 7 (41) (2015) 17244–17248.
[38] Y. Wang, X.H. Liu, J.L. Zhang, D. Aili, B. Liedberg, Time-resolved botulinum neurotoxin A activity monitored using peptide-functionalized Au nanoparticle energy transfer sensors, Chem. Sci. 5 (7) (2014) 2651–2656.
[39] M.M. Li, J. Li, H.X. Di, H.Q. Liu, D.B. Liu, Live-cell pyrophosphate imaging by in situ hot-spot generation, Anal. Chem. 89 (6) (2017) 3532–3537.
[40] W. Zhou, Q. Li, H.Q. Liu, J. Yang, D.B. Liu, Building electromagnetic hot spots in living cells via target-triggered nanoparticle dimerization, ACS Nano 11 (4) (2017) 3532–3541.
[41] X.Q. Ren, Q.W. Zhang, J.L. Yang, X.J. Zhang, X.M. Zhang, Y.T. Zhang, L.P. Huang, C.S. Xu, Y.C. Ge, H. Chen, X.H. Liu, Y. Wang, Dopamine imaging in living cells and retina by surface-enhanced Raman scattering based on functionalized gold nanoparticles, Anal. Chem. 93 (31) (2021) 10841–10849.
[42] W. Haiss, N.T.K. Thanh, J. Aveyard, D.G. Fernig, Determination of size and concentration of gold nanoparticles from UV–Vis spectra, Anal. Chem. 79 (11) (2007) 4215–4221.
[43] M. Mathlouthi, A.M. Seuvre, J.L. Koenig, F.t.-i.r. and laser-Raman spectra of adenine and adenosine, Carbohydr. Res. 131 (1) (1984) 1–15.
[44] E.K. Marshall, A rapid clinical method for the estimation of urea in urine, J. Biol. Chem. 14 (4) (1913) 283–290.

[45] Y.F. Zheng, G.W. Xu, J. Yang, X.J. Zhao, T. Pang, H.W. Kong, Determination of urinary nucleosides by direct injection and coupled-column high-performance liquid chromatography, J. Chromatogr. B. 819 (1) (2005) 85–90.
[46] E. Rodriguez-Gonzalo, D. Garcia-Gomez, R. Carabias-Martinez, Development and validation of a hydrophilic interaction chromatography-tandem mass spectrometry method with on-line polar extraction for the analysis of urinary nucleosides. Potential application in clinical diagnosis, J. Chromatogr. A 1218 (50) (2011) 9055–9063.
[47] W.Y. Hsu, C.J. Chen, Y.C. Huang, F.J. Tsai, L.B. Jeng, C.C. Lai, Urinary nucleosides as biomarkers of breast, colon, lung, and gastric cancer in Taiwanese, PLoS ONE 8 (12) (2013) 8.
[48] S. Huang, L. Wang, W. Chen, S. Feng, J. Lin, Z. Huang, G. Chen, B. Li, R. Chen, Potential of non-invasive esophagus cancer detection based on urine surface-enhanced Raman spectroscopy, Laser Phys. Lett. 11 (11) (2014).
[49] L. Ma, Z. Zhang, X. Li, Non-invasive disease diagnosis using surface-enhanced Raman spectroscopy of urine and saliva, Appl. Spectrosc. Rev. 55 (3) (2020) 197–219.
[50] M. Bylesjo, M. Rantalainen, O. Cloarec, J.K. Nicholson, E. Holmes, J. Trygg, OPLS discriminant analysis: combining the strengths of PLS-DA and SIMCA classification, J. Chemometr. 20 (8–10) (2006) 341–351.
[51] L. Bervoets, G. Massa, W. Guedens, E. Louis, J.-.P. Noben, P. Adriaensens, Metabolic profiling of type 1 diabetes mellitus in children and adolescents: a case-control study, Diabetol. Metab. Syndrome 9 (2017).
[52] J. Lin, Z. Huang, X. Lin, Q. Wu, K. Quan, Y. Cheng, M. Zheng, J. Xu, Y. Dai, H. Qiu, D. Lin, S. Feng, Rapid and label-free urine test based on surface-enhanced Raman spectroscopy for the non-invasive detection of colorectal cancer at different stages, Biomed. Opt. Express 11 (12) (2020) 7109–7119.
[53] B. Callejon-Leblic, T. Garcia-Barrera, A. Pereira-Vega, J.Luis Gomez-Ariza, Metabolomic study of serum, urine and bronchoalveolar lavage fluid based on gas chromatography mass spectrometry to delve into the pathology of lung cancer, J. Pharm. Biomed. Anal. 163 (2019) 122–129.